Numerical analysis of high frequency surface acoustic wave chemical and biological sensors based on multilayered Diamond/AlN/$LiNbO_3$ substrates

Subramanian K.R.S. Sankaranarayanan and Venkat R. Bhethanabotla
Sensors Research Laboratory, Department. of Chemical and Biomedical Engineering.
University of South Florida, Tampa, Florida, 33620, USA

Abstract

We have used 3-D coupled field structural finite element models to study the acoustic wave propagation characteristics of diamond/AlN/$LiNbO_3$ multi-layered piezoelectric surface acoustic wave devices for applications in chemical and biological sensing. These devices were studied as a method to increase device frequency and sensitivity, and maintain standard fabrication procedures. Although recent experimental investigations have realized GHz frequency devices based on such multilayered substrates, very little is known about the acoustic wave propagation characteristics in these devices. Identifying the optimum configuration and thickness of the various layers involved still represents a challenge which is addressed in this work.

1. Introduction

Surface acoustic wave (SAW) devices that operate at high GHz frequencies, present low insertion loss, and retain superior performance are critical for chemical & biological sensing as well as for communications applications. The operating frequency of SAW devices is directly proportional to the substrate's acoustic wave velocity and inversely proportional to the spatial periodicity of the interdigital transducers (IDTs). This makes the fabrication of GHz frequency devices based on bare substrates such as $LiNbO_3$ difficult as it requires submicron or nanometric IDTs, which are difficult to achieve using standard lithographic techniques.

Most of the recent research has focused on advanced SAW filters and sensors based on multilayered structures which could allow for operational frequencies in the GHz frequency range[1]. The operating frequency of SAW devices is directly proportional to the substrate's acoustic wave velocity; hence the highest acoustic wave velocity material (diamond) is needed for fabrication of GHz frequency devices. The aluminum nitride piezoelectric layer also has a very high acoustic wave velocity and a fairly large piezoelectric coupling coefficient along its c-axis, in comparison to other piezoelectric materials. Hence, the highest frequency SAW devices can be expected on diamond substrates with an aluminum nitride piezoelectric layer. This would make it possible to realize GHz frequency devices with standard transducer configurations. Although recent experimental investigations have realized GHz frequency devices based on such multilayered substrates, very little is known about the acoustic wave propagation characteristics in these devices. Identifying the optimum configuration (Fig. 1) and thickness of the various layers involved still represents a challenge[2].

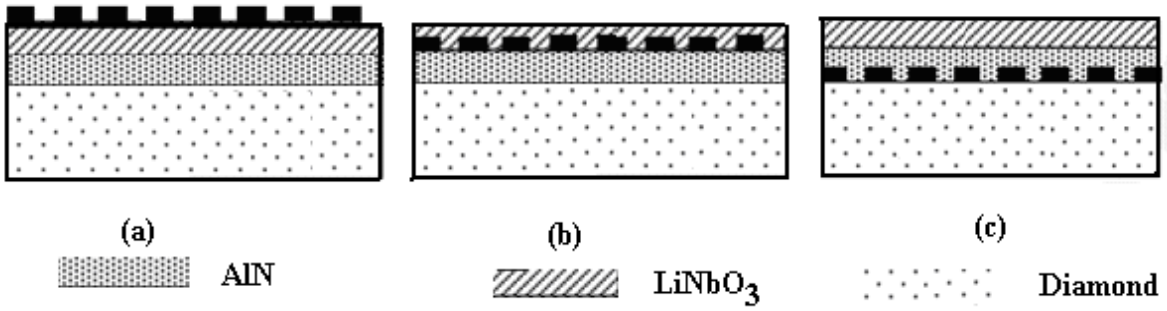

Figure 1. Examples of configurations (a) IDT/$LiNbO_3$/AlN/diamond (b) $LiNbO_3$/IDT/AlN/diamond and (c) $LiNbO_3$/AlN/IDT/diamond.

The models commonly used to simulate the mechanical and electrical behavior of piezoelectric transducers, to study acoustic wave propagation, generally introduce simplifying assumptions that are often invalid for actual designs[3]. The geometries of practical transducers are often two (2-D) or three dimensional (3-D)[4, 5]. Simulations of piezoelectric media require the complete set of fundamental equations relating mechanical and electrical quantities to be solved. Finite difference or finite element schemes are sufficient to handle the differential equations[6-11]. The finite element method has been preferred because it allows handling of complex geometries and multilayered composite structures. Our previous investigations also indicate the feasibility of the finite element models to study acoustic wave propagation in piezoelectric devices[9-11].

In the present work, we use 3-D coupled field structural finite element models to study the acoustic wave propagation characteristics in these multilayered piezoelectric SAW devices based on diamond for potential applications in chemical and biological sensing. The displacement and voltage waveforms obtained for varying thicknesses of diamond, AlN and $LiNbO_3$ substrates are analyzed to understand acoustic wave propagation characteristics in multilayered substrates. The feasibility of achieving GHz frequency devices using SAW devices based on diamond layer is investigated in this work.

2. Theory

The propagation of acoustic waves in piezoelectric materials is governed by the mechanical equations of motion and Maxwell's equations for electrical behavior[12-14]. The constitutive equations of piezoelectric media in linear range coupling the two are given by:

$$T_{ij} = c^{E}_{ijkl} S_{kl} - e^{t}_{kij} E_k \qquad [1]$$

$$D_i = e_{ikl} S_{kl} + \varepsilon^{S}_{ik} E_k \qquad [2]$$

In the above equations, T_{ij} represent the components of stress, c_{ijkl}^{E} the elastic constant for constant electric field, S_{kl} the strain, E_k the electric field intensity, D_i the electric displacement, e_{kij}^{t} the piezoelectric constant, and ε_{ik}^{S} the permittivity for constant strain. The acoustic wave propagation velocity is five orders of magnitude smaller than that of electromagnetic waves. Therefore, the quasistatic assumptions help reduce Maxwell's equation to $\frac{\partial D_i}{\partial x_i} = 0$ and $E_i = -\frac{\partial \phi}{\partial x_i}$, where φ represents the electric potential. The components of strain are defined by

$$S_{ij} = \frac{1}{2}\left(\frac{\partial u_i}{\partial x_j} + \frac{\partial u_j}{\partial x_i} \right) \qquad [3]$$

The equation of motion in the absence of internal body forces is given as

$$\frac{\partial T_{ij}}{\partial x_j} - \rho \frac{\partial^2 u_i}{\partial t^2} = 0 \qquad [4]$$

where ρ is the density and u_i represent the components of displacement. Substituting and rearranging the above set of equations leads to a system of four coupled wave equations for the electric potential and the three component of displacement in piezoelectric materials which are solved for the piezoelectric substrate or the solid domain:

$$-\rho \frac{\partial^2 u_i}{\partial t^2} + c_{ijkl}^{E} \frac{\partial^2 u_k}{\partial x_j \partial x_l} + e_{kij} \frac{\partial^2 \phi}{\partial x_k \partial x_j} = 0 \qquad [5]$$

$$e_{ikl} \frac{\partial^2 u_k}{\partial x_i \partial x_l} - \varepsilon_{ik}^{s} \frac{\partial^2 \phi}{\partial x_i \partial x_k} = 0 \qquad [6]$$

These coupled wave equations can be discretized and solved for generating displacement profiles and voltages at each element/node using the finite element method[15].

3. Computational details

A. Model parameters

A coupled field finite element structural model is utilized to study the acoustic wave propagation in diamond/AlN/IDT/$LiNbO_3$ layered SAW devices. The 3-D FE model describes two-port structures based on configurations depicted in Fig. 1. The simulated device consists of three finger pairs in each port. The fingers are considered as mass-less electrodes to ignore the second-order effects arising from electrode mass, thereby

simplifying computation. The periodicity of the finger pairs i.e. λ is 40 microns and the aperture width is 200 microns. The transmitting and receiving IDT's are spaced 130 microns or 3.25λ apart. The simulated SAW device dimensions are 20 λ in propagation length and 12.5 λ wide. The thickness of the diamond film was kept constant at 1 λ, whereas AlN thickness was taken as λ/8. By varying the thickness of $LiNbO_3$ from 1 λ to 10 λ, the relative ratios of the thickness of the three films were varied and the propagation characteristics of the acoustic wave as well as the dispersion relationship in the multi-layered substrate configuration shown in Fig. 1 (b) were studied. The simulated models have a total of approx. 250,000 nodes and are solved for four degrees of freedom (three displacements and voltage). The model was created to have the highest densities throughout the surface and middle of the substrate. The simulated voltage and displacement profiles obtained at the output IDT's are used to measure wave attenuation and velocity changes and thereby optimize the thickness of the waveguide, *i.e.* the diamond and AlN layer.

B. Structure excitation

Two types of analysis are carried out for each of the three devices, *i.e.*, pure $LiNbO_3$ and diamond/AlN/IDT/$LiNbO_3$ with thickness ratios 1:0.125:10 and 1:0.125:1.

(1) An impulse input of 10 V over 1 ns is applied to study the frequency response of the device.

(2) AC analysis with a 5 V peak-peak input and 100 MHz frequency to study the wave propagation characteristics in the multilayered substrates.

4. Results and discussion

A. Impulse response analysis

By applying an impulse function as an input, the frequency response can be calculated [5]. For the impulse response analysis, it is important that we scan a sufficient range of frequencies up to the GHz range. Hence, the structure was simulated for a total of 200 ns, with a time step of 0.5 ns. The time step of sampling utilized, *i.e.*, 0.5 ns, determines the highest frequency which can be obtained when we perform our frequency response analysis. The highest frequency which can be sampled is $\frac{1}{2*0.5e-9}$ which corresponds to 1.0 GHz. The total time of 200 ns similarly determines the lowest frequency which can be sampled. The lowest frequency which can be sampled is $\frac{1}{2*200e-9}$ which corresponds to 2.5 MHz. The center frequency of the device is properly sampled using the above chosen time step and simulation time.

The calculated frequency response for an input impulse (1 ns) of 10 V applied on a pure $LiNbO_3$ substrate is shown in Fig. 2. Since the propagation velocity on a $LiNbO_3$ substrate is around 3,500 m/s, the center frequency of the SAW device is ~100 MHz for an IDT finger spacing of 10 micrometers. When the simulations are

performed for the multilayered substrates, the frequency response obtained is very different from that for a pure $LiNbO_3$ substrate. In particular, for both the multilayered substrates, there are acoustic modes which propagate at velocities higher than that possible on a pure $LiNbO_3$ substrate.

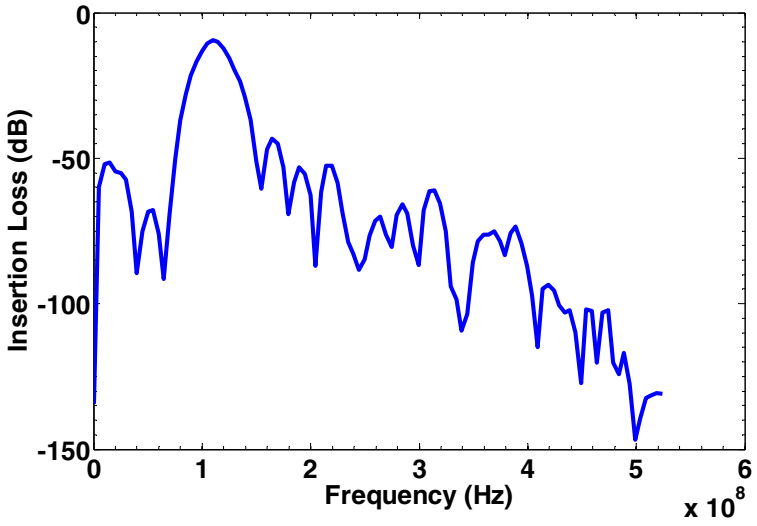

Figure 2. Simulated frequency response for a SAW device based on a pure $LiNbO_3$ substrate. The center frequency of the device corresponds to approx. 100 MHz.

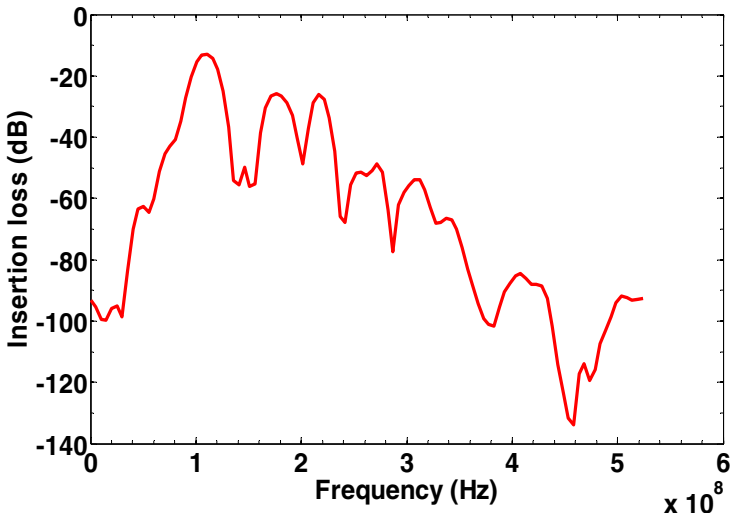

Figure 3. Simulated frequency response for a multilayered SAW device based on diamond/AlN/IDT/$LiNbO_3$ configuration. The thickness ratio of diamond/AlN/IDT/$LiNbO_3$ is 1:0.125:1. The simulated frequency of the device shows peaks corresponding to approx. 120, 180 and 220 MHz. The center frequency of the device is approx. 100 MHz. The acoustic wave modes corresponding to the higher frequencies have similar insertion losses.

The excitation of a multilayered piezoelectric substrate results in generation of multiple wave modes as seen in Figs. 3 and 4. For all the wave modes, the simulation results indicate a decrease in phase velocity with increasing $LiNbO_3$ film thickness. When the thickness ratio of diamond/AlN/IDT/$LiNbO_3$ is 1:0.125:10, it can be seen that three Rayleigh waves are excited within the structure with phase velocities of 3,500 m/s for the zeroth mode, 8,300 m/s for the first mode and 12,300 m/s for the phase velocity of the second mode, approaching the Rayleigh

wave of pure diamond. For the optimized substrate thicknesses, it is thus possible to have the third Rayleigh mode as the dominant mode thereby allowing the wave to propagate entirely in the diamond substrate. It can also be seen that when the thickness ratio of diamond/AlN/IDT/$LiNbO_3$ is 1:0.125:1, the insertion loss of the device is reduced for all the three modes when compared to diamond/AlN/IDT/$LiNbO_3$ thickness ratio of 1:0.125:10.

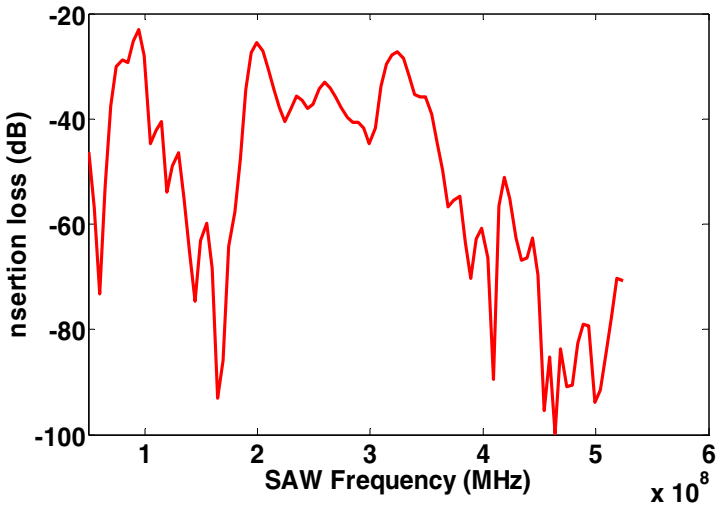

Figure 4. Simulated frequency response for a SAW device based on a diamond/AlN/IDT/$LiNbO_3$ configuration. The thickness ratio of diamond/AlN/IDT/$LiNbO_3$ is 1:0.125:10. The simulated frequency of the device shows peaks corresponding to approx. 100, 200 and 320 MHz. The acoustic wave modes corresponding to the three frequencies have similar insertion losses.

B. AC response analysis

The application of an AC electrical signal on the input transducer fingers results in generation of a mechanical wave which then propagates towards the output transducer fingers. The coupled field finite element model developed in the present study is able to capture the generation and propagation of SAWs on multilayered piezoelectric substrate as shown in Figs. 5-8.

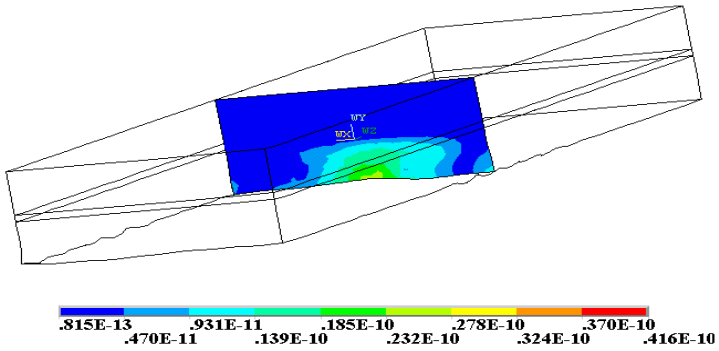

Figure 5. The displacement contours along the substrate depth obtained at t=75 ns in a multilayered SAW device based on diamond/AlN/IDT/$LiNbO_3$ with a finger periodicity of 40 μm and for the 10V applied input AC voltage. The thickness ratio of diamond/AlN/IDT/$LiNbO_3$ is 1:0.125:10. The scale bar shown above represents the displacement amplitudes of SAW in meters. It can be seen that the wave propagated primarily in the $LiNbO_3$ substrate.

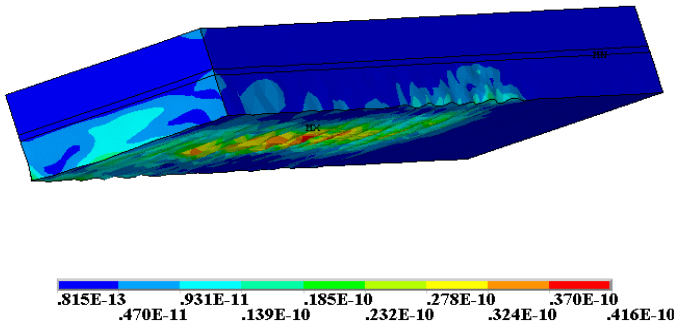

Figure 6. The displacement contours obtained at t=75 ns in a multilayered SAW device based on diamond/AlN/IDT/$LiNbO_3$ with a finger periodicity of 40 μm and for the 10 V applied input AC voltage. The thickness ratio of diamond/AlN/IDT/$LiNbO_3$ is 1:0.125:10. The scale bar shown above represents the displacement amplitudes of SAW in meters.

Our simulated displacement profiles along the longitudinal, surface normal and shear horizontal directions indicate that Rayleigh waves propagate in the multilayered configurations. Analysis of the particle displacement profiles along the depth of multilayered diamond/AlN/IDT/$LiNbO_3$ substrates at different locations along the SAW delay path was also carried out to investigate the acoustic energy confinement in multilayered SAW devices for the simulated device design parameters.

For diamond/AlN/IDT/$LiNbO_3$ thickness ratio of 1:0.125:10; we find that the acoustic energy is primarily confined in the *$LiNbO_3$* layer as shown in Fig. 5, and hence the acoustic wave propagates along surface of the $LiNbO_3$ substrate (Fig. 6). At these thickness ratios, we find that the acoustic velocity attained is not very high (approx. 4,100 m/s) and hence this configuration cannot be utilized to attain the GHz frequencies for the

simulated IDT periodicity. On the other hand, when the thickness ratios of diamond/AlN/IDT/$LiNbO_3$ is changed to 1:0.125:1 by reducing the $LiNbO_3$ thickness, the acoustic energy is confined primarily in the diamond and AlN layers as shown in Fig. 7. At higher simulation times, the wave is also partly radiated into the *$LiNbO_3$* layer in the form of bulk waves, thereby increasing the insertion loss of the device.

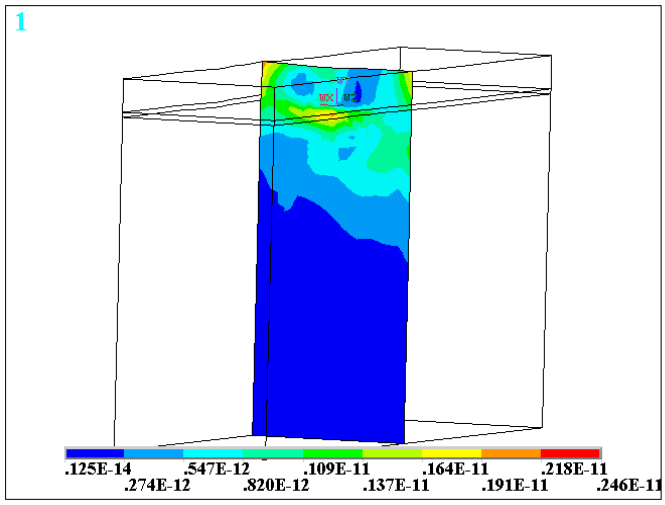

Figure 7. The displacement contours along the substrate depth obtained at t=30 ns in a multilayered SAW device based on diamond/AlN/IDT/$LiNbO_3$ with a finger periodicity of 40 μm and for the 10 V applied input AC voltage. The thickness ratio of diamond/AlN/IDT/$LiNbO_3$ is 1:0.125:1. The scale bar shown above represents the displacement amplitudes of SAW in meters. It can be seen that the wave propagated primarily in the diamond substrate.

We find that the acoustic wave modes propagating in the diamond film (Fig. 8) attains very high velocities close to 12,300 m/s, thereby indicating the possibility of fabricating GHz frequency devices. Simulations of additional devices with varying $LiNbO_3$ thickness in the range 1 to 10 λ to obtain optimum normalized thicknesses are in progress in order to confirm the high potential of the new diamond/AlN/IDT/$LiNbO_3$ structures for high-performance and high-frequency SAW devices. Efforts are also underway to utilize the optimized configurations in fluid-solid interaction FE model to investigate the influence of fluid loading on Rayleigh wave propagation in multi-layered SAW devices and evaluate their potential use in chemical and biosensing applications.

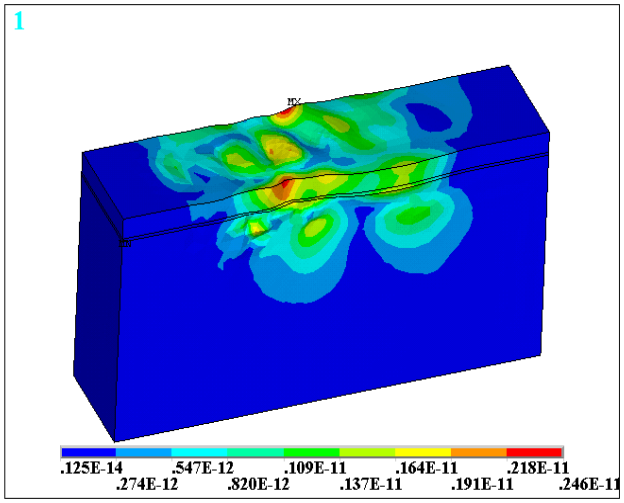

Figure 8. The displacement contours along the substrate depth obtained at t=30 ns in a multilayered SAW device based on diamond/AlN/IDT/$LiNbO_3$ with a finger periodicity of 40 µm and for the 10 V applied input AC voltage. The thickness ratio of diamond/AlN/IDT/$LiNbO_3$ is 1:0.125:1. The scale bar shown above represents the displacement amplitudes of SAW in meters.

5. Limitations of Finite Element Simulations

A fine mesh generation is required for accurate modeling of a SAW device. The modeling of acoustic wave propagation in multilayered substrates requires at least 20 first order elements per wavelength in each of the different substrates. Hence, much higher node densities are required to model a device approaching practical dimensions. Also, the simulations are time consuming. Simulation time will increase with increasing mesh density. Another major setback arises from acoustic wave reflection from the edges if the simulations are carried out for sufficiently longer times. One of the ways to overcome this limitation would be employment of damping elements at the ends of the substrate. While longer simulation times are necessary to attain a stable state, too long a simulation time results in wave reflections causing instabilities to set in. A simulation time of 200 ns was found to be optimum for the substrate dimensions considered in the present study.

6. Conclusions

We have simulated the acoustic wave propagation in high frequency devices based on multilayered diamond based substrates. We find that the acoustic wave propagation is dictated by relative thickness of the various substrates. Upon varying the thickness ratio of diamond: AlN: $LiNbO_3$ from 1:0.125:1 to 1:0.125:10, our simulation results indicate that the wave propagation shifts preferentially from propagation in $LiNbO_3$ to that in diamond. Frequency response analyses of these multilayered substrates indicate the possibility of fabricating a GHz frequency device for substrate thickness ratios when the acoustic wave propagates primarily in the diamond substrate. When the thickness of the diamond layer is smaller compared to that of $LiNbO_3$ substrate, then device frequency is as high as 320 MHz. This latter result illustrates the greatest advantage of using diamond as an acoustic substrate. It allows the fabrication of SAW devices operating in the gigahertz frequency range using

standard optical lithography. Efforts are underway to simulate more thickness in the range 1 to 10 λ to optimize the substrate thickness to develop higher frequency devices near the GHz range with lesser insertion loss.

Nomenclature:

$\boldsymbol{T}$ – Vector of Mechanical stresses

$\boldsymbol{S}$ – Vector of Mechanical strains

$\boldsymbol{E}$ – Vector of Electric field

$\boldsymbol{D}$ – Vector of Dielectric displacement

$\boldsymbol{c}^{E}$ – Mechanical stiffness matrix for constant electric field E.

$\boldsymbol{\varepsilon}^{s}$– Permittivity matrix for constant mechanical strain

$\boldsymbol{e}$ – Piezoelectric matrix

$\boldsymbol{\varphi}$ –Electric potential function

$\boldsymbol{u}$ - Displacement

ρ – Substrate density

t – Time

Acknowledgments

The authors wish to thank the Engineering Computing Center at USF for providing the computational facilities. The authors thank Reetu Singh of USF for useful discussions. This work was supported in part by NSF grants DGE-0221681, CHE-0722887 and ECCS-0801929, US Army Research Contract No. W81XWH-05-1-0585 and the USF Office of Research by an interdisciplinary research grant.

References

1 E. Dogheche, D. Remiens, S. Shikata, A. Hachigo, and H. Nakahata, Appl. Phys. Letts. **87**, 213503/1 (2005).

2 P. Kirsch, M. B. Assouar, O. Elmazria, V. Mortet, and P. Alnot, Appl. Phys. Letts. **88**, 223504/1 (2006).

3 D. P. Morgan, in *IEEE International Frequency Control Symposium*, (1998), p. 439.

4 R. Lerch, in *Circuits and Systems, IEEE International Symposium*, (1988), Vol. 2, p. 1399

5 R. Lerch, Ultrasonics, Ferroelectrics and Frequency Control, IEEE Transactions **37**, 233 (1990).

6 G. Xu, Smart Materials and Structures **9**, 973 (2000).

7 M. Z. Atashbar, B. J. Bazuin, M. Simpeh, and S. Krishnamurthy, Sensors and Actuators, B: Chemical **B111-112**, 213 (2005).

8 S. J. Ippolito, K. Kalantar-Zadeh, D. A. Powell, and W. Wlodarski, in *IEEE Ultrasonics Symposium*, (2003), p. 1.

[9] S. K. R. S. Sankaranarayanan and V. R. Bhethanabotla, in *AIChE Annual Conference*, Salt Lake City, Utah, (2007), p. 1.

[10] S. K. R. S. Sankaranarayanan, V. R. Bhethanabotla, and B. Joseph, ECS Transactions (19, Acoustic Wave Based Sensors and Sensor Systems), 19 (2006).

[11] S. K. R. S. Sankaranarayanan, V. R. Bhethanabotla, and B. Joseph, in *IEEE Sensors Symposium*, Atlanta, GA, (2007), p. 1.

[12] B. A. Auld, *Acoustic Fields and Waves in Solids.* vol. I (John Wiley and Sons, New York, N.Y. USA, 1973).

[13] B. A. Auld, *Acoustic Fields and Waves in Solids.* vol. II (John Wiley and Sons, New York, N.Y., USA, 1973).

[14] D. S. Ballantine, R. M. White, S. J. Martin, A. J. Ricco, G. C. Frye, E. T. Zellers, and H. Wohltjen, *Acoustic Wave Sensors: Theory, Design, and Physico-Chemical Applications.* (Academic Press, New York, N.Y. USA. 1997).

[15] Computer code ANSYS, v. 10 (ANSYS Inc. www.ansys.com)